A Finite-Dimensional Nonanalytic Spectral Transition and Exact High-Fidelity Rate–Distortion for Rank-r Born Prediction on Complex Grassmannians

Lluis Eriksson

August 13, 2026

Abstract

Let P be Haar on the complex Grassmannian $\mathrm{Gr}_{\mathbb{C}}(r, d)$ and set $\rho_P = P/r$. We solve two coupled finite-dimensional problems. First, on the sphere of traceless Hermitian external fields with fixed Frobenius norm, we determine incompatible weak- and strong-field optimizers of the matrix-Bingham free energy $\log \mathbb{E} e^{s\,\mathrm{tr}(AP)}$. For $1 < r < d/2$, an exact cubic Haar moment and a uniform C^2 perturbation theorem make the positive one-spike spectrum uniquely optimal at weak field. A parameter-uniform differentiated Grassmann Laplace expansion upgrades the strong-field Ky Fan limit to exact eventual uniqueness of the rank-r two-block spectrum. The globally optimized free energy must therefore fail to be real analytic at a finite field; at its first exit from the one-spike branch there is either nonconjugate coexistence or transverse-Hessian degeneracy. The balanced case $r = d/2$ is selected by a negative quartic coefficient instead.

Second, we determine the unrestricted classical Shannon rate–distortion function for squared-Frobenius reconstruction of ρ_P on a nonempty open interval adjacent to zero distortion. Arbitrary standard-Borel classical memories and arbitrary reports reduce by conditional least squares to the full posterior-density body, not merely to the source Grassmannian. Exact eventual two-block optimality and radial localization reduce the complete Shannon dual to one variable. If $M_{d,r}(\kappa) = \mathbb{E} e^{\kappa\,\mathrm{tr}(PQ)}$, $m = (\log M_{d,r})'$, and $b = (dm - r^2)/[r(d - r)]$, then for all sufficiently large κ,

$$D = \frac{d-r}{rd}(1 - b^2), \qquad \mathcal{R} = \kappa m - \log M_{d,r}.$$

The frontier is attained by a covariant matrix-Bingham channel whose posterior mean is a depolarized rank-r projector. A Jacobi–Selberg calculation gives the exact high-rate constant, and complementation transfers the result to every nontrivial rank. The complete intermediate-phase classification and the full all-distortion rank-r curve remain open.

1 Introduction

Matrix-Bingham laws on Stiefel and Grassmann manifolds are classical objects in directional statistics, shape analysis, and subspace learning [1, 2, 3, 4, 5]. Their normalizers are unitary orbital integrals, equivalently confluent hypergeometric functions of matrix argument, with a theory going back to James and Constantine [6, 7]. Harish–Chandra–Itzykson–Zuber formulas, Schur expansions, Weingarten calculus, deficient-rank representations, and sampling algorithms are also established [8, 9, 10, 11].

The inverse problem studied here is different: at fixed trace and Frobenius norm, which external spectrum maximizes the Grassmann matrix-Bingham normalizer, and what does that maximization imply for unrestricted rate–distortion? Schur convexity does not answer the first question because the constraint sphere is not a majorization chain [12]. Standard Grassmann quantization does not answer the second because optimal calibrated Born reports range over a convex body of mixed states rather than over the source orbit alone [13, 14, 15, 16]. Exact invariant source-coding formulas on compact groups and spheres provide important comparators but do not perform this posterior-body optimization [17, 18].

For $1 < r < d/2$ there cannot be one field-independent spectral ansatz. Weak fields select a positive one-spike spectrum. Strong fields select a spectrum with r equal positive and $d-r$ equal negative eigenvalues. We first prove that this mismatch forces a finite-dimensional nonanalyticity in the optimized free energy. We then strengthen strong-field convergence to exact eventual optimality and use it to solve the unrestricted Shannon problem on a complete high-fidelity interval.

The main contributions are:

1. exact quadratic and cubic invariant moments, plus the balanced quartic selector and all equality cases;

2. exact weak-field one-spike rigidity, canonical-branch reversal, and a finite-dimensional nonanalytic spectral transition;

3. a parameter-uniform differentiated Grassmann Laplace theorem, including explicit chart density, differentiated tail bounds, and stability under internal block collisions;

4. exact eventual rank-r two-block uniqueness at fixed radius and exact eventual optimization over the full physical posterior-density body;

5. covariant Bingham attainment of the unrestricted high-fidelity rate–distortion frontier and exact posterior-mean self-consistency; and

6. the sharp Jacobi–Selberg high-rate constant and complementary-rank transfer.

This article is self-contained and supersedes both unpublished rank-r drafts from which it developed: the preliminary spectral-transition manuscript and the separate high-fidelity manuscript. Neither draft should be cited separately. No theorem here depends on an unpublished companion. Table 1 records the mathematical scope across ranks and makes clear which stronger all-distortion claims are not part of this paper.

Table 1: Exact scope of the unified theorem package across rank regimes.

Rank regime	Results proved here	Boundary not claimed here
$r = 1$	high-fidelity specialization and sharp constant	complete all-distortion curve, thermodynamic limit, and minimax layer
$1 < r < d/2$	exact weak one-spike phase, exact eventual rank-r phase, finite nonanalyticity, and high-fidelity RDF	intermediate spectral phases and the complete all-distortion curve
$r = d/2$	exact balanced weak selector and high-fidelity RDF	a forced weak/strong branch exchange is not asserted
$d/2 < r < d$	exact transfer by projector complementation	no independent phase classification is required

2 Orbital and operational formulations

Let $1 \le r \le d-1$, let $P_r = \operatorname{diag}(I_r, 0_{d-r})$, and let $P = UP_rU^\dagger$ for Haar $U \in U(d)$. For a traceless Hermitian field A and $s \in \mathbb{R}$, define

$$Z_{d,r}(s,A) = \mathbb{E}e^{s\,\operatorname{tr}(AP)}, \qquad F_{d,r}(s,A) = \log Z_{d,r}(s,A). \tag{1}$$

On the fixed-radius sphere

$$\mathcal{S}_R = \{A = A^\dagger : \operatorname{tr} A = 0,\ \|A\|_F = R\},$$

write $\Phi_{d,r,R}(s) = \max_{A\in\mathcal{S}_R} F_{d,r}(s,A)$.

Proposition 2.1 (Classical normalizer and complement symmetry)**.** *With the standard complex matrix-argument convention,*

$$Z_{d,r}(s,A) = {}_1F_1^{(1)}(r;d;sA), \qquad Z_{d,d-r}(s,A) = Z_{d,r}(-s,A) \quad (\operatorname{tr} A = 0). \tag{2}$$

Proof. Schur–Weyl duality and the unitary Schur integral give

$$Z_{d,r}(s,A) = \sum_{m\ge 0}\frac{s^m}{m!}\sum_{\lambda\vdash m} f^\lambda \frac{s_\lambda(1^r)}{s_\lambda(1^d)} s_\lambda(A).$$

In the complex convention $C_\lambda^{(1)} = f^\lambda s_\lambda$ and $s_\lambda(1^r)/s_\lambda(1^d) = (r)_\lambda^{(1)}/(d)_\lambda^{(1)}$, which is the defining series for ${}_1F_1^{(1)}$. If P is Haar of rank r, then $I-P$ is Haar of rank $d-r$ and $\operatorname{tr}[A(I-P)] = -\operatorname{tr}(AP)$, proving the second identity. □

Now normalize the source state as

$$\rho_P = \frac{P}{r}, \qquad S_P = \rho_P - \frac{I}{d}, \qquad R_0^2 = \|S_P\|_F^2 = \frac{d-r}{rd}.$$

Lemma 2.2 (Posterior-report reduction)**.** *For any standard-Borel classical memory Z and square-integrable Hermitian report $\widehat{\rho}_Z$, replacing the report by $\sigma_Z = \mathbb{E}(\rho_P \mid Z)$ cannot increase distortion or mutual information. The exact physical reproduction body is*

$$\mathcal{C}_{d,r} = \operatorname{conv}\{P/r : P \in \operatorname{Gr}_{\mathbb{C}}(r,d)\} = \{\sigma \succeq 0 : \operatorname{tr}\sigma = 1,\ \sigma \preceq I/r\}. \tag{3}$$

Conversely every point of this body is a finite mixture of source states.

Proof. Conditional expectation is the Hilbert–Schmidt L^2 projection, so

$$\mathbb{E}\|\rho_P - \widehat{\rho}_Z\|_F^2 = \mathbb{E}\|\rho_P - \sigma_Z\|_F^2 + \mathbb{E}\|\sigma_Z - \widehat{\rho}_Z\|_F^2.$$

The replacement is a deterministic function of Z, so data processing applies. Equation (3) is the standard majorization description of the convex hull of a unitary orbit. □

Writing $A = \sigma - I/d$, the unrestricted rate–distortion function is

$$\mathcal{R}_{d,r}(D) = \inf\{I(P;Z) : \mathbb{E}\|S_P - A_Z\|_F^2 \le D\}.$$

For $\lambda \ge 0$, define

$$\begin{aligned} Q_\lambda(A) &= \mathbb{E}e^{-\lambda\|S_P - A\|_F^2} \\ &= e^{-\lambda(R_0^2 + \|A\|_F^2)} Z_{d,r}(2\lambda/r, A). \end{aligned} \tag{4}$$

Lemma 2.3 (Shannon–Gibbs converse and equality)**.** *For every admissible report channel,*

$$I(P;A) + \lambda \mathbb{E}\|S_P - A\|_F^2 \geq -\log \sup_{a \in \mathcal{C}_{d,r} - I/d} Q_\lambda(a). \tag{5}$$

Equality holds when, for almost every used report a,

$$\frac{\mathrm{d}P_{P|A=a}}{\mathrm{d}\mu}(P) = \frac{e^{-\lambda\|S_P - a\|_F^2}}{Q_\lambda(a)}$$

and Q_λ is constant on the report support.

Proof. Disintegrate mutual information as the average $D(P_{P|A=a}\|\mu)$. Nonnegativity of relative entropy relative to the displayed Gibbs law gives the pointwise inequality; integration and $Q_\lambda(a) \leq \sup Q_\lambda$ prove (5). The stated conditions are exactly the equality conditions. □

3 Exact weak-field geometry

Put $X_A = \mathrm{tr}(AP)$. The first shape-sensitive term is explicit.

Lemma 3.1 (Quadratic and cubic Haar moments)**.** *For traceless Hermitian A and $d > 2$,*

$$\mathbb{E}X_A = 0, \tag{6}$$

$$\mathbb{E}X_A^2 = \frac{r(d-r)}{d(d^2-1)}\,\mathrm{tr}(A^2), \tag{7}$$

$$\mathbb{E}X_A^3 = \frac{2r(d-r)(d-2r)}{d(d^2-1)(d^2-4)}\,\mathrm{tr}(A^3). \tag{8}$$

Proof. Invariant polynomials of degrees two and three on the traceless Hermitian subspace are multiples of $\mathrm{tr}\,A^2$ and $\mathrm{tr}\,A^3$. Evaluate at $A_0 = |e_1\rangle\langle e_1| - I/d$. Since $\langle e_1, Pe_1\rangle \sim \mathrm{Beta}(r, d-r)$, its variance and third central moment give (7)–(8) after division by $\mathrm{tr}\,A_0^2 = (d-1)/d$ and $\mathrm{tr}\,A_0^3 = (d-1)(d-2)/d^2$. □

Define the canonical fields

$$A_{1,R} = \frac{R}{\sqrt{d(d-1)}}\,\mathrm{diag}(d-1, -1, \ldots, -1), \tag{9}$$

$$A_{r,R} = \frac{R}{\sqrt{dr(d-r)}}\,\mathrm{diag}((d-r)I_r, -rI_{d-r}). \tag{10}$$

Theorem 3.2 (Exact weak-field selection)**.** *Let $d > 2$, $1 \leq r < d/2$, and $R > 0$. For all sufficiently small $s > 0$, the unique maximizing orbit of $F_{d,r}(s,\cdot)$ on $\mathcal{S}_R$ is $U(d)\cdot A_{1,R}$.*

Proof. Uniformly with two ambient derivatives on $\mathcal{S}_R$,

$$F_{d,r}(s,A) = c_2R^2s^2/2 + c_3s^3\,\mathrm{tr}(A^3)/6 + O_{C^2}(s^4),$$

and $c_3 > 0$. A Lagrange-multiplier calculation shows that every stationary spectrum of $\mathrm{tr}\,A^3$ has at most two values. If the larger value has multiplicity k, then

$$\mathrm{tr}\,A^3 = R^3\frac{d-2k}{\sqrt{dk(d-k)}},$$

which is uniquely maximal at $k = 1$. At the one-spike $x > y$, the constrained second variation transverse to its conjugacy orbit is $3(y-x)\sum_{i>1} v_i^2 < 0$. Compact separation away from the orbit and uniform C^2 convergence preserve both global separation and strict transverse concavity for small s. □

When $d = 2r$, complement symmetry removes all odd terms.

Proposition 3.3 (Balanced quartic selector)**.** *For $d = 2r \geq 4$,*

$$\mathbb{E}X_A^4 = c_{22,d}(\operatorname{tr} A^2)^2 + c_{4,d} \operatorname{tr} A^4, \qquad c_{4,d} = -\frac{3d}{8(d-3)(d-1)(d+1)(d+3)} < 0. \tag{11}$$

Consequently $A_{r,R}$ is the unique weak-field maximizing orbit.

Proof. Appendix B derives (11) by exact Schur characters. The fourth cumulant differs from the fourth moment by a quantity constant on $\mathcal{S}_R$. Since $\operatorname{tr} A^4 \geq R^4/d$, equality forces $d/2$ entries $R/\sqrt{d}$ and $d/2$ entries $-R/\sqrt{d}$. Its constrained Hessian is strictly positive, so the negative quartic selector and the same C^2 perturbation argument prove the claim. □

4 Strong-field transition and exact eventual phase

Let $h_r(A) = \sum_{i=1}^r \lambda_i^{\downarrow}(A)$.

Lemma 4.1 (Uniform compact Laplace principle)**.** *Uniformly for $A \in \mathcal{S}_R$,*

$$s^{-1} F_{d,r}(s, A) \longrightarrow h_r(A).$$

Moreover

$$\max_{A \in \mathcal{S}_R} h_r(A) = R\sqrt{\frac{r(d-r)}{d}}, \tag{12}$$

with unique maximizing orbit $U(d) \cdot A_{r,R}$.

Proof. Ky Fan's principle identifies $h_r(A) = \max_{P \in \mathrm{Gr}_{\mathbb{C}}(r,d)} \operatorname{tr}(AP)$. A fixed-radius Grassmann ball around a maximizing plane has center-independent positive Haar mass, giving matching uniform exponential upper and lower bounds. If the top r eigenvalues sum to S, Cauchy's inequality on the top and bottom blocks gives $R^2 \geq S^2/r + S^2/(d-r)$, with equality only when both blocks are constant. □

The next result is the analytic core that converts convergence into exact eventual rigidity. Its proof is expanded in Appendix A.

Lemma 4.2 (Uniform differentiated Grassmann Laplace expansion)**.** *Let $N \subset \mathcal{S}_R$ be represented by a compact set of labeled diagonal spectra with $a_i - a_j \geq \delta > 0$ for $i \leq r < j$. Uniformly with all ordinary spectral derivatives of order at most two on an open gap neighborhood of N,*

$$\log Z_{d,r}(s, A) = s h_r(A) - n \log s + C_{d,r} - \sum_{i \leq r < j} \log(a_i - a_j) + O_{C^2(N)}(s^{-1}), \qquad n = r(d-r). \tag{13}$$

The expansion remains smooth under eigenvalue collisions within either block.

Theorem 4.3 (Exact eventual two-block optimizer)**.** *For every $1 \leq r \leq d/2$ and $R > 0$, there is a finite $u_*(d, r)$ such that*

$$\operatorname*{argmax}_{A \in \mathcal{S}_R} Z_{d,r}(s, A) = U(d) \cdot A_{r,R} \qquad (sR > u_*(d, r)). \tag{14}$$

The threshold is independent of R after the scaling sR.

Proof. The compact Laplace principle localizes every global maximizer in a fixed neighborhood of the unique Ky Fan orbit. Use labeled diagonal spectral coordinates with the top-r index set fixed. On the trace-zero sphere,

$$\mathrm{Hess}_{\mathcal{S}_R}\, h_r(A)[v,v] = -\frac{h_r(A)}{R^2}\|v\|_2^2,$$

which is uniformly negative in a sufficiently small neighborhood of $A_{r,R}$. Lemma 4.2 makes every remaining Hessian uniformly $O(1)$, so $\log Z$ is strictly geodesically concave there for large sR. The two-block orbit is stationary for every s by its within-block permutation symmetry. Strict local concavity plus global localization proves exact uniqueness. □

For $1 < r < d/2$, the weak and strong optimizers differ. Their support slopes are

$$h_r(A_{1,R}) = \frac{R(d-r)}{\sqrt{d(d-1)}}, \qquad h_r(A_{r,R}) = R\sqrt{\frac{r(d-r)}{d}},$$

and the second is strictly larger.

Theorem 4.4 (Finite-dimensional nonanalytic transition)**.** *Let $d \geq 5$ and $1 < r < d/2$. Then:*

(i) the one-spike orbit is the unique global maximizer on a weak-field interval;

(ii) the rank-r two-block orbit is the exact unique global maximizer on a strong-field interval;

(iii) the two canonical real-analytic branches cross at least once; and

(iv) the optimized envelope $\Phi_{d,r,R}$ fails to be real analytic at some finite $s > 0$.

At the first exit from one-spike uniqueness there is either a nonconjugate coexisting global maximizer or loss of negative definiteness of the one-spike transverse Hessian.

Proof. Theorem 3.2 and Theorem 4.3 prove (i) and (ii). The canonical comparator inequality reverses between the two intervals, so continuity proves (iii). On a nonempty interval adjacent to zero, $\Phi_{d,r,R} = F_{d,r}(s, A_{1,R})$. If Φ were real analytic on $(0,\infty)$, the identity theorem would continue this equality everywhere, contradicting (ii). At the supremum of the one-spike uniqueness interval, if neither coexistence nor Hessian degeneracy occurred, compact global separation and strict local concavity would persist to a larger interval, a contradiction. □

The theorem does not assert a first-order transition, a unique transition, or the absence of intermediate or re-entrant spectral strata.

For $d/2 < r < d-1$, projector complementation gives $F_{d,r}(s,A) = F_{d,d-r}(s,-A)$. Hence the weak optimizer is the negative one-spike, the exact eventual optimizer is $A_{r,R}$, and the same nonanalyticity and first-exit conclusions hold. The endpoint $r = d-1$ reduces to the rank-one geometry under this sign change.

The two canonical branches used for exact replay have closed normalizers:

$$Z_{d,r}(s, A_{1,R}) = \exp\left[-\frac{sRr}{\sqrt{d(d-1)}}\right] {}_1F_1\left(r; d; sR\sqrt{\frac{d}{d-1}}\right), \tag{15}$$

$$Z_{d,r}(s, A_{r,R}) = \exp\left[-sRr\sqrt{\frac{r}{d(d-r)}}\right] {}_1F_1^{(1)}\left(r; d; sR\sqrt{\frac{d}{r(d-r)}}I_r\right). \tag{16}$$

The displayed matrix argument in (16) is padded by $d-r$ zero eigenvalues in the standard stability convention.

Proposition 4.5 (The transition occurs in the physical report body). *Let $1 < r < d/2$ and*

$$0 < R \le R_{\text{phys}} := \frac{d-r}{r\sqrt{d(d-1)}}.$$

Both $I/d + A_{1,R}$ and $I/d + A_{r,R}$ lie in $\mathcal{C}_{d,r}$. On the compact fixed-radius physical section

$$\{A \in \mathcal{S}_R : I/d + A \in \mathcal{C}_{d,r}\},$$

the one-spike is uniquely optimal at weak field, the rank-r block is exactly uniquely optimal at strong field, and the optimized physical envelope fails to be real analytic at least once.

Proof. The one-spike eigenvalue constraints $-1/d \le a_i \le (d-r)/(rd)$ give precisely the displayed radius bound; the rank-r block is physical for every $R \le R_0$, and $R_{\text{phys}} \le R_0$. The weak-field optimizer is unique even on the larger sphere. The differentiated Laplace theorem and strict concavity prove exact strong-field uniqueness on the larger sphere, hence on the physical section. The analytic identity argument of Theorem 4.4 then applies verbatim to the physical envelope. □

5 Radial optimization over the physical body

Return to the density normalization $A = \sigma - I/d$. Uniformly on the compact physical body, (4) gives

$$\lambda^{-1} \log Q_\lambda(A) \longrightarrow -R_0^2 - R^2 + \frac{2}{r} h_r(A) \le -(R - R_0)^2, \qquad R = \|A\|_F. \tag{17}$$

At a fixed radius R, equality in the last spectral inequality is attained at

$$A = \frac{R}{R_0} S_Q. \tag{18}$$

After optimizing over R as well, equality in the limiting expression forces $R = R_0$ and hence $A = S_Q$. This separates the two equality statements that are sometimes conflated.

Uniform convergence localizes all large-λ maximizing radii to $[R_0/2, R_0]$. Theorem 4.3 then applies uniformly and forces every optimizer to have the form $A = bS_Q$, $0 < b \le 1$. Put

$$\kappa = \frac{2\lambda b}{r^2}, \qquad M_{d,r}(\kappa) = \mathbb{E} e^{\kappa \operatorname{tr}(PQ)}, \qquad m_{d,r}(\kappa) = (\log M_{d,r})'(\kappa). \tag{19}$$

On this orbit the dual partition is exactly

$$Q_\lambda(bS_Q) = e^{-\lambda R_0^2(1+b^2) - 2\lambda b/d} M_{d,r}(\kappa). \tag{20}$$

Radial stationarity is exactly

$$b = b_{d,r}(\kappa) := \frac{d\, m_{d,r}(\kappa) - r^2}{r(d-r)}, \qquad b'_{d,r}(\kappa) = \frac{d}{r(d-r)} \operatorname{Var}_\kappa(\operatorname{tr}(PQ)) > 0. \tag{21}$$

Proposition 5.1 (Jacobi–Selberg normalizer). *For $r \le d/2$ and $n = r(d-r)$,*

$$M_{d,r}(\kappa) = e^{\kappa r} K_{d,r} \kappa^{-n} \big(1 + O(e^{-c\kappa} \operatorname{poly} \kappa)\big), \qquad K_{d,r} = \prod_{j=0}^{r-1} \frac{\Gamma(d-r+j+1)}{\Gamma(j+1)}. \tag{22}$$

The remainder estimate is stable under every fixed number of κ-derivatives.

Proof. The nonzero eigenvalues x_i of PQP have density proportional to $\prod_i (1-x_i)^{d-2r} \prod_{i<j} (x_i - x_j)^2$ on $[0,1]^r$. Substitute $x_i = 1 - y_i/\kappa$. The ratio of the limiting Laguerre–Selberg integral to the original Jacobi–Selberg normalization is $K_{d,r}$. Extending $[0,\kappa]^r$ to $[0,\infty)^r$ gives an exponentially small polynomially weighted tail. Each κ-derivative changes only the polynomial weight, so the same exponential tail controls all fixed derivative orders. □

Equation (22) gives

$$m_{d,r}(\kappa) = r - \frac{n}{\kappa} + O(\kappa^{-2}), \qquad b_{d,r}(\kappa) = 1 - \frac{d}{\kappa} + O(\kappa^{-2}). \tag{23}$$

Uniformly for b near one, the radial second derivative is $-2\lambda R_0^2 + O(1)$, so it is strictly negative for sufficiently large λ. Localization excludes the lower endpoint and the derivative at $b = 1$ points inward.

Theorem 5.2 (Exact eventual Shannon-dual optimizer)**.** *There exists $\lambda_*(d, r) < \infty$ such that for every $\lambda > \lambda_*(d, r)$ the supremum in* (5) *is attained on one unitary orbit bS_Q, where $b \in (0, 1)$ is the unique solution of* (21) *with $\kappa = 2\lambda b/r^2$.*

Proof. Equation (17) localizes every global maximizer to the fixed annulus. Theorem 4.3 then reduces the spectral optimization exactly to (20). Its derivative vanishes precisely at (21). The uniform negative second derivative, the inward derivative at $b = 1$, and exclusion of the lower annular boundary give one and only one radial maximum. Unitary covariance leaves exactly its conjugacy orbit. □

6 Exact high-fidelity rate–distortion

Let Q be Haar and define the covariant channel

$$\frac{\mathrm{d}p_\kappa(P \mid Q)}{\mathrm{d}\mu(P)} = \frac{e^{\kappa \operatorname{tr}(PQ)}}{M_{d,r}(\kappa)}. \tag{24}$$

Covariance makes the P marginal Haar. Block symmetry yields

$$\mathbb{E}(P \mid Q) = \frac{m}{r}Q + \frac{r-m}{d-r}(I - Q), \qquad \mathbb{E}(\rho_P \mid Q) = b_{d,r}(\kappa)\frac{Q}{r} + (1 - b_{d,r}(\kappa))\frac{I}{d}. \tag{25}$$

Thus the dual optimizer is exactly the posterior mean of its attaining channel.

Theorem 6.1 (Exact unrestricted high-fidelity frontier)**.** *For every $1 \le r \le d/2$ there is $D_*(d, r) > 0$ such that, for $0 < D < D_*(d, r)$, the unrestricted classical Shannon rate–distortion function of the Haar source P/r is parametrized by all sufficiently large κ as*

$$D_{d,r}(\kappa) = \frac{d-r}{rd}\big(1 - b_{d,r}(\kappa)^2\big), \tag{26}$$

$$\mathcal{R}_{d,r}(D_{d,r}(\kappa)) = \kappa m_{d,r}(\kappa) - \log M_{d,r}(\kappa). \tag{27}$$

The channel (24) *attains the infimum.*

Proof. Theorem 5.2 evaluates the unrestricted Shannon converse. On every used report orbit, (24) is the Gibbs equality kernel and Q_λ is constant. Equations (21) and (25) show that each report equals its own posterior mean. Hence all equality conditions in Lemma 2.3 hold. Posterior-mean orthogonality gives (26); integrating the log likelihood ratio gives (27). Since $b'(\kappa) > 0$, distortion decreases strictly, and the large-κ tail covers a nonempty open interval adjacent to zero. □

Corollary 6.2 (Sharp high-rate constant)**.** *For $n = r(d - r)$,*

$$\mathcal{R}_{d,r}(D) = n \log \frac{2(d-r)}{rD} - n - \log K_{d,r} + o(1), \qquad D \downarrow 0. \tag{28}$$

All logarithms and rates are in nats.

Proof. Equations (22) and (23) give $D = 2(d-r)/(r\kappa) + O(\kappa^{-2})$ and $\mathcal{R} = n\log\kappa - n - \log K_{d,r} + O(\kappa^{-1})$. Eliminate κ. The coefficient n is half the real dimension $2r(d-r)$, while the displayed additive constant is the sharper result. □

Proposition 6.3 (Complementary-rank transfer)**.** *For every* $1 \le r \le d-1$,

$$\mathcal{R}_{d,r}(D) = \mathcal{R}_{d,d-r}\left(\frac{r^2}{(d-r)^2}D\right). \tag{29}$$

Thus Theorem 6.1 applies to every nontrivial rank after explicit distortion rescaling.

Proof. The map $P \mapsto I - P$ preserves Haar measure and

$$\frac{I-P}{d-r} - \frac{I}{d} = -\frac{r}{d-r}\left(\frac{P}{r} - \frac{I}{d}\right).$$

The same affine bijection maps the posterior-mean bodies, preserves mutual information, and multiplies squared Frobenius distortion by $r^2/(d-r)^2$. □

7 The diagnostic case $d = 5, r = 2$

The first unbalanced rank-two case connects the transition and information frontier with exact low-dimensional formulas. At radius $R = 1$, direct Gauss–Jacobi quadrature gives the canonical-branch crossing

$$s_\times = 4.858579052914\ldots, \qquad F_{5,2}(s_\times, A_{1,1}) = F_{5,2}(s_\times, A_{2,1}) = 0.606942410196\ldots.$$

This is a comparator crossing, not a claimed location of the global nonanalytic point and not an exclusion of intermediate spectra.

For the high-fidelity branch define

$$I_j(\kappa) = \int_0^1 u^j e^{-\kappa u}\,\mathrm{d}u = \frac{j!}{\kappa^{j+1}}\left(1 - e^{-\kappa}\sum_{\ell=0}^{j}\frac{\kappa^\ell}{\ell!}\right).$$

The Jacobi density gives the exact scalar normalizer

$$M_{5,2}(\kappa) = 72e^{2\kappa}\big(I_3(\kappa)I_1(\kappa) - I_2(\kappa)^2\big). \tag{30}$$

Table 2: Deterministic rank-two Bingham-channel replay. The theorem identifies these values with the unrestricted RDF only after the existential high-fidelity threshold has been entered.

κ	$b_{5,2}$	$\kappa(1-b_{5,2})$	D	I (nats)
20	0.7500056	4.9998880	0.1312475	7.0047226
40	0.8750000	5.0000000	0.0703125	11.1634634
80	0.9375000	5.0000000	0.0363281	15.3223465

8 Born-probability interpretation

Let Y be an independent Haar query ray and allow a classical memory Z to report an arbitrary square-integrable field $q(Z,Y)$. Conditional least squares replaces it by $\mathrm{tr}(\sigma_Z|Y\rangle\langle Y|)$ without increasing loss. For the traceless difference $X = \rho_P - \sigma_Z$, the projective second moment gives

$$\mathbb{E}_Y\,\mathrm{tr}(X|Y\rangle\langle Y|)^2 = \frac{\mathrm{tr}(X^2)}{d(d+1)}. \tag{31}$$

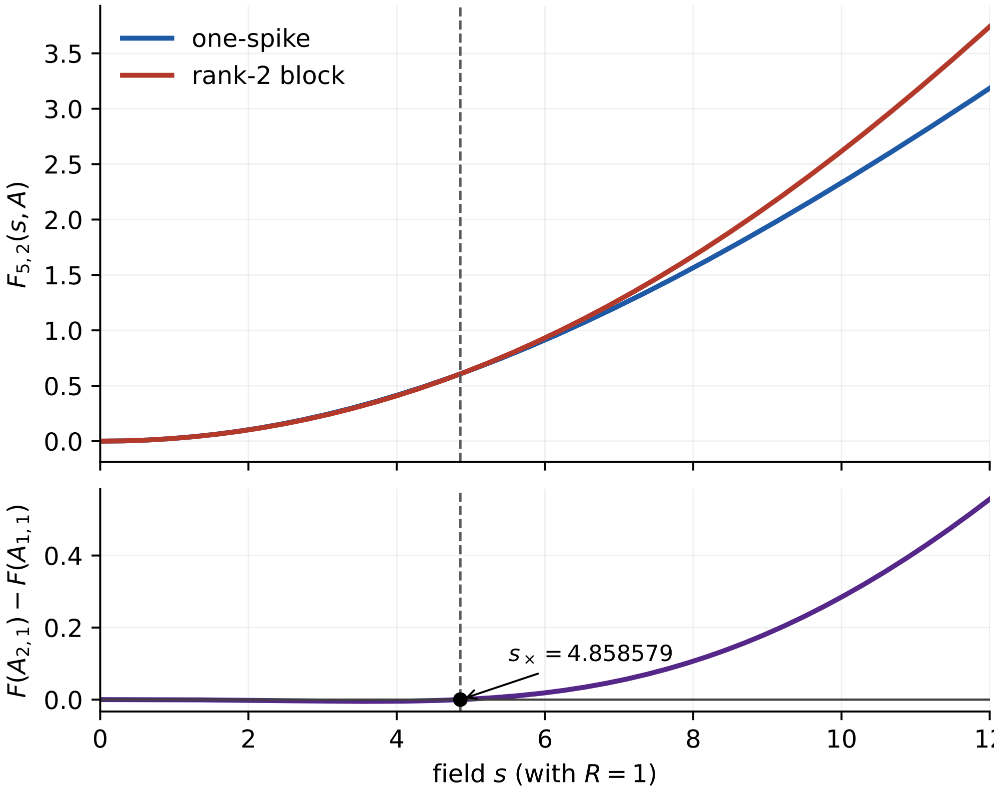

Figure 1: Exact canonical branches for $d = 5$, $r = 2$, and $R = 1$. The lower panel is their difference. The figure replays the proved branch reversal but is not a premise of Theorem 4.4.

Consequently Theorem 6.1 is the exact high-fidelity information–accuracy frontier for the complete rank-r Born-probability field after $D = d(d+1)\varepsilon_2$. Any weighted complex projective 2-design replaces the Haar query average exactly [19].

This is a theorem about calibrated probability prediction with classical memory. It does not derive Born's rule, establish intrinsic randomness of click sequences, supply a state-update law, or identify particle dynamics.

9 Relation to prior work and open boundary

The Bingham family, matrix-hypergeometric normalizer, Jacobi law, Selberg integrals, Grassmann quantization, and local dimension law are established. Fixed-spectrum large-dimensional spherical-integral transitions are also known [20, 21, 22]. Here the nonanalyticity is produced at fixed finite d by optimizing the external spectrum, and the information theorem additionally optimizes over the full physical radius and reproduction body.

For $r = 1$, the formulas above give the projective high-fidelity specialization and agree with the established qubit real-sphere reduction [18]; a complete all-distortion rank-one curve, thermodynamic limit, worst-state formulation, and finite-block theory are not claimed here. For $r > 1$, the paper incorporates the complete mathematical content of the two unpublished rank-r drafts into a self-contained proof of exact eventual strong-field uniqueness and the operational Shannon frontier.

Three substantive problems remain open. The proof does not compute a universal numerical value of $D_*(d, r)$, classify intermediate spectral strata or reentrance, or determine the complete all-distortion rank-r RDF. Those questions require a global finite-field spectral classification beyond the asymptotic intervals proved here.

10 Conclusion

The fixed-radius and operational problems now form one chain. Exact weak-field moments select a one-spike spectrum; differentiated strong-field Laplace asymptotics select the rank-r block exactly; their incompatibility forces a finite-dimensional nonanalyticity; radial localization then converts the strong phase into the exact unrestricted high-fidelity Shannon frontier. The attaining Bingham channel is posterior-mean self-consistent, and the Jacobi–Selberg normalizer supplies the exact additive high-rate constant. The self-contained unified statement therefore explains both why scalarization fails at intermediate fields and why it becomes rigorously exact near perfect fidelity.

Reproducibility statement

The frozen replay archive contains four lightweight deterministic scripts: exact low-degree invariant identities, bounded spectral diagnostics, the $d = 5, r = 2$ canonical-branch figure generator, and the high-fidelity normalization/RDF verifier through $d = 18$. Run from the archive directory:

```
python verify_grassmann_crossover.py
python verify_grassmann_spectral_switch.py --d 5 --r 2
python generate_d5r2_example.py
python verify_high_fidelity_grassmann_rdf.py
```

The frozen archive is

`Eriksson_Unified_Grassmann_Transition_RDF_Replay_v1.zip`

with SHA-256

`5bf74b40a90534c5ceff2ecfc7bacfefb05e6436928bae3a3fc52fbb465acb86.`

It is distributed alongside the submission PDF in the frozen release bundle. No public locator is asserted in this version before deposition; the filename and digest above identify the archive byte for byte. These checks verify constants and conventions; no numerical computation is used as a substitute for a global-optimality proof.

Acknowledgements

OpenAI Codex assisted with symbolic checks, literature triage, and adversarial proof review. The author retains responsibility for every claim.

A Differentiated Grassmann Laplace expansion

This appendix supplies the detailed uniform argument behind Lemma 4.2. It is included because exact eventual optimality, rather than mere convergence, depends on two differentiated orders.

A.1 A fixed graph chart and the Haar density

Split $\mathbb{C}^d = \mathbb{C}^r \oplus \mathbb{C}^{d-r}$ according to the top-r eigenspace of a labeled diagonal field $A = \mathrm{diag}(A_+, A_-)$. Every plane transverse to the second summand is the graph of $W \in \mathbb{C}^{(d-r)\times r}$, with orthogonal projector

$$P(W) = \begin{pmatrix} I \\ W \end{pmatrix} (I + W^\dagger W)^{-1} \begin{pmatrix} I & W^\dagger \end{pmatrix}. \tag{32}$$

In these coordinates Haar probability is

$$d\mu(P(W)) = c_{d,r} \det(I + W^\dagger W)^{-d} \, dW, \tag{33}$$

where dW is Lebesgue measure on $2r(d-r)$ real coordinates. Both the projector and density are analytic on every bounded chart ball.

Let K be a compact set of spectra contained in the cross-gap region $a_i - a_j \geq \delta$ for $i \leq r < j$. Choose one chart radius $\rho > 0$ for all $a \in K$. From (32), uniformly with two ordinary a-derivatives,

$$\operatorname{tr}(AP(W)) = h_r(a) - \sum_{i \leq r < j} (a_i - a_j)|W_{ji}|^2 + E_a(W), \qquad |\partial_a^\alpha E_a(W)| \leq C\|W\|^4 \quad (|\alpha| \leq 2). \tag{34}$$

Because the phase is linear in a, the estimates for positive derivative order are in fact simpler than the zeroth-order bound; the displayed common form is convenient for differentiating the exponential.

A.2 Uniform exterior control

The unique maximizing plane for every $a \in K$ is $W = 0$. Joint compactness gives $c_0 > 0$ such that the phase is at most $h_r(a) - c_0$ outside the fixed chart. Each of at most two a-derivatives of the integrand contributes a factor bounded by $C(1+s)^2$. Hence the differentiated exterior integral is $O(s^2 e^{-c_0 s}) e^{s h_r(a)}$ uniformly.

Inside the chart, shrink ρ so that $|E_a(W)| \leq (\delta/4)\|W\|^2$. On $s^{-2/5} \leq \|W\| \leq \rho$, the phase loss is at least $(\delta/4)s^{-4/5}$. After multiplication by s, this annulus and its first two derivatives contribute

$$O\big(s^2 e^{-c_1 s^{1/5}}\big) e^{s h_r(a)}, \tag{35}$$

again smaller than every inverse power of s. These bounds also control derivatives of the discarded domain because the cutoff radii are independent of a.

A.3 Gaussian rescaling with two derivatives

On $\|W\| \leq s^{-2/5}$ put $W = s^{-1/2}V$. The real Jacobian contributes s^{-n}, $n = r(d-r)$, and (34) becomes

$$s\big(\operatorname{tr}(AP(s^{-1/2}V)) - h_r(a)\big) = -\sum_{i \leq r < j} (a_i - a_j)|V_{ji}|^2 + s^{-1} E_{4,a}(V) + O(s^{-2}\|V\|^6).$$

The density (33) has a parallel expansion $1 + s^{-1} J_2(V) + O(s^{-2}\|V\|^4)$. Expand the product through order s^{-1} before differentiating. For $|\alpha| \leq 2$, every derivative is bounded by

$$C_\alpha (1 + \|V\|^{m_\alpha}) \exp[-(\delta/2)\|V\|^2], \tag{36}$$

uniformly in $a \in K$ and large s. Dominated convergence and Taylor's theorem with integral remainder therefore give

$$Z_{d,r}(s, A) = e^{s h_r(a)} s^{-n} c_{d,r} \prod_{i \leq r < j} (a_i - a_j)^{-1} \big(1 + s^{-1} L_1(a) + O_{C^2(K)}(s^{-2})\big). \tag{37}$$

The complex Gaussian normalization is the product of the reciprocal cross-gaps. Taking a logarithm of (37) proves (13).

Only cross-block gaps occur in (34), (36), and the determinant in (37). Eigenvalues may collide arbitrarily within the top or bottom block without changing the chart, the unique maximizing plane, or any denominator. This proves the claimed internal-collision stability.

B Schur-character derivation of the balanced fourth moment

For every positive integer m, Schur–Weyl integration gives

$$\mathbb{E}(\operatorname{tr}(AP))^m = \sum_{\lambda \vdash m} f^\lambda \frac{s_\lambda(1^r)}{s_\lambda(1^d)} s_\lambda(a_1, \dots, a_d). \tag{38}$$

At $m = 4$ and $p_1 = 0$, the character formula leaves only cycle types (4) and $(2, 2)$:

$$\begin{aligned} s_{(4)} &= p_2^2/8 + p_4/4, & s_{(3,1)} &= -p_2^2/8 - p_4/4, \\ s_{(2,2)} &= p_2^2/4, & s_{(2,1,1)} &= -p_2^2/8 + p_4/4, \\ s_{(1,1,1,1)} &= p_2^2/8 - p_4/4. \end{aligned}$$

The hook-content formula gives

$$\begin{aligned} s_{(4)}(1^n) &= \frac{n(n+1)(n+2)(n+3)}{24}, & s_{(3,1)}(1^n) &= \frac{n(n-1)(n+1)(n+2)}{8}, \\ s_{(2,2)}(1^n) &= \frac{n^2(n^2-1)}{12}, & s_{(2,1,1)}(1^n) &= \frac{n(n+1)(n-1)(n-2)}{8}, \\ s_{(1,1,1,1)}(1^n) &= \frac{n(n-1)(n-2)(n-3)}{24}. \end{aligned}$$

Writing $q_\lambda = s_\lambda(1^r)/s_\lambda(1^d)$, the coefficients obtained from (38) are

$$\begin{aligned} c_{22} &= \frac{1}{8}\big(q_{(4)} - 3q_{(3,1)} + 4q_{(2,2)} - 3q_{(2,1,1)} + q_{(1,1,1,1)}\big), \\ c_4 &= \frac{1}{4}\big(q_{(4)} - 3q_{(3,1)} + 3q_{(2,1,1)} - q_{(1,1,1,1)}\big). \end{aligned}$$

The symmetric-group dimensions used in these combinations are

$$(f^{(4)}, f^{(3,1)}, f^{(2,2)}, f^{(2,1,1)}, f^{(1,1,1,1)}) = (1, 3, 2, 3, 1)$$

Setting $r = d/2$ now yields

$$c_{22,d} = \frac{3(d^2-6)}{16(d-3)(d-1)(d+1)(d+3)}, \qquad c_{4,d} = -\frac{3d}{8(d-3)(d-1)(d+1)(d+3)},$$

which is Proposition 3.3.

References

[1] John T. Kent. “The Complex Bingham Distribution and Shape Analysis”. In: *J. R. Stat. Soc. B* 56.2 (1994), pp. 285–299. DOI: 10.1111/j.2517-6161.1994.tb01978.x.

[2] Muhammad Ali, Junbin Gao, and Michael Antolovich. “Parametric Classification of Bingham Distributions Based on Grassmann Manifolds”. In: *IEEE Transactions on Image Processing* 28.12 (2019), pp. 5771–5784. DOI: 10.1109/TIP.2019.2922100.

[3] Armine Bagyan and Donald Richards. “Complete Asymptotic Expansions for the Normalizing Constants of High-Dimensional Matrix Bingham and Matrix Langevin Distributions”. In: *Symmetry, Integrability and Geometry: Methods and Applications* 20 (2024), p. 094. DOI: 10.3842/SIGMA.2024.094. arXiv: 2402.08663.

[4] Lu Wei and Tianxi Ji. “Asymptotic Matrix-Variate Bingham Distributions and Privacy-Preserving Principal Component Analysis”. In: *IEEE Transactions on Signal Processing* 73 (2025), pp. 1966–1978. DOI: 10.1109/TSP.2025.3569636.

[5] Luca Cazzella, Soren Hauberg, Georgios Arvanitidis, and Matteo Matteucci. “On the Latent Information Geometry of the Grassmann Manifold”. In: *Proceedings of the 29th International Conference on Artificial Intelligence and Statistics*. 2026. URL: https://openreview.net/forum?id=BhLHFZwMEr.

[6] Alan T. James. “Distributions of Matrix Variates and Latent Roots Derived from Normal Samples”. In: *The Annals of Mathematical Statistics* 35.2 (1964), pp. 475–501. DOI: 10.1214/aoms/1177703550.

[7] A. G. Constantine. “Some Non-Central Distribution Problems in Multivariate Analysis”. In: *The Annals of Mathematical Statistics* 34.4 (1963), pp. 1270–1285. DOI: 10.1214/aoms/1177703863.

[8] C. Itzykson and J.-B. Zuber. “The Planar Approximation. II”. In: *Journal of Mathematical Physics* 21.3 (1980), pp. 411–421. DOI: 10.1063/1.524438.

[9] Benoît Collins and Piotr Śniady. “Integration with Respect to the Haar Measure on Unitary, Orthogonal and Symplectic Group”. In: *Communications in Mathematical Physics* 264.3 (2006), pp. 773–795. DOI: 10.1007/s00220-006-1554-3. arXiv: math-ph/0402073.

[10] Alexei Onatski. “Detection of Weak Signals in High-Dimensional Complex-Valued Data”. In: *Random Matrices: Theory and Applications* 3.1 (2014), p. 1450001. DOI: 10.1142/S2010326314500014. arXiv: 1207.7098.

[11] Jonathan Leake, Colin McSwiggen, and Nisheeth K. Vishnoi. “Sampling Matrices From Harish-Chandra–Itzykson–Zuber Densities With Applications to Quantum Inference and Differential Privacy”. In: *Random Structures & Algorithms* 67 (2025), e70030. DOI: 10.1002/rsa.70030. arXiv: 2011.05417.

[12] Suvrit Sra. “On Inequalities for Normalized Schur Functions”. In: *European Journal of Combinatorics* 51 (2016), pp. 492–494. DOI: 10.1016/j.ejc.2015.07.005.

[13] Bishwarup Mondal, Rupak Dutta, and Robert W. Heath, Jr. “Quantization on the Grassmann Manifold”. In: *IEEE Transactions on Signal Processing* 55.8 (2007), pp. 4208–4216. DOI: 10.1109/TSP.2007.896112.

[14] Wei Dai, Youjian Liu, and Brian Rider. “Quantization Bounds on Grassmann Manifolds and Applications to MIMO Communications”. In: *IEEE Transactions on Information Theory* 54.3 (2008), pp. 1108–1123. DOI: 10.1109/TIT.2007.915691. arXiv: cs/0603039.

[15] Renaud-Alexandre Pitaval, Lu Wei, Olav Tirkkonen, and Jukka Corander. “Volume of Metric Balls in High-Dimensional Complex Grassmann Manifolds”. In: *IEEE Transactions on Information Theory* 62.9 (2016), pp. 5105–5116. DOI: 10.1109/TIT.2016.2594289. arXiv: 1508.00256.

[16] Erwin Riegler, Günther Koliander, and Helmut Bölcskei. “Lossy Compression of General Random Variables”. In: *Information and Inference: A Journal of the IMA* 12.3 (2023), pp. 1759–1829. DOI: 10.1093/imaiai/iaac035. arXiv: 2111.12312.

[17] Peter Harremoës. “Maximum Entropy on Compact Groups”. In: *Entropy* 11.2 (2009), pp. 222–237. DOI: 10.3390/e11020222. arXiv: 0901.0015.

[18] Alex Dytso and Martina Cardone. “Uniform Distribution on the $(n-1)$-Sphere: Rate–Distortion under Squared Error Distortion”. In: *2024 IEEE International Symposium on Information Theory.* 2024. arXiv: 2401.04248.

[19] Aidan Roy and A. J. Scott. “Weighted Complex Projective 2-Designs from Bases: Optimal State Determination by Orthogonal Measurements”. In: *Journal of Mathematical Physics* 48.7 (2007), p. 072110. DOI: 10.1063/1.2748617. arXiv: quant-ph/0703025.

[20] Alice Guionnet and Ofer Zeitouni. “Large Deviations Asymptotics for Spherical Integrals”. In: *Journal of Functional Analysis* 188.2 (2002), pp. 461–515. DOI: 10.1006/jfan.2001.3833.

[21] Alice Guionnet and Mylène Maïda. “A Fourier View on the R-Transform and Related Asymptotics of Spherical Integrals”. In: *Journal of Functional Analysis* 222.2 (2005), pp. 435–490. DOI: 10.1016/j.jfa.2004.09.015. arXiv: math/0406121.

[22] Alice Guionnet and Jonathan Husson. “Asymptotics of k Dimensional Spherical Integrals and Applications”. In: *ALEA: Latin American Journal of Probability and Mathematical Statistics* 19 (2022), pp. 769–797. DOI: 10.30757/ALEA.v19-30. arXiv: 2101.01983.